Valorization of AZ91 by the hydrolysis reaction for hydrogen production (Electrochemical approach)

Serge Al Bacha, Isabelle Aubert, Mirvat Zakhour, Michel Nakhl, Jean-Louis Bobet

ARTICLE IN PRESS
JID: JMAA [m5+;March 2, 2021;20:3]
Available online at www.sciencedirect.com
ScienceDirect
Journal of Magnesium and Alloys xxx (xxxx) xxx
www.elsevier.com/locate/jma

Valorization of AZ91 by the hydrolysis reaction for hydrogen production (Electrochemical approach)

S. Al Bacha[a,b], I. Aubert[c], M. Zakhour[a], M. Nakhl[a], J.L. Bobet[b,*]

[a] *LCPM/PR$_2$N (EDST), Lebanese University, Faculty of Science II, 90656 Jdeidet El Metn, Lebanon*
[b] *Université de Bordeaux, ICMCB, CNRS, UMR 5026, F-33600 Pessac, France*
[c] *University of Bordeaux, CNRS, Arts et Métiers, Institute of technology, Bordeaux INP, INRAE, I2M Bordeaux, F-33400 Talence, France*

Received 24 September 2020; received in revised form 11 November 2020; accepted 6 December 2020
Available online xxx

Abstract

The hydrolysis of Mg-based materials appears to be an ideal solution for clean energy production. Green hydrogen was produced by the hydrolysis reaction of a "standard" AZ91 alloy (called AZ91 in the following) in "model" seawater solution. Two milling speeds (*i.e.* 250 rpm and 350 rpm) were tested to enhance the reactivity of AZ91. Graphite and $AlCl_3$ were used as ball milling additives. Milling at higher rotational speed is more energetic, hence it ameliorates the most the hydrolysis performance of AZ91. Comparing both milling additives, $AlCl_3$ enhances the most the hydrolysis of AZ91 with a generation of 65% of its theoretical H_2 generation capacity. The best material was obtained by milling AZ91 at 350 rpm with graphite for 2 h followed by a further milling with $AlCl_3$ for 2 h – a yield of 75% of its theoretical H_2 generation capacity was reached within a few minutes. The corrosion behavior of milled AZ91 was investigated by anodic polarization and electrochemical impedance spectroscopy (EIS). The calculated electrochemical parameters from EIS fitting of two materials milled under different conditions but with the same milling additive are approximately the same. This suggests that, in order to fully evaluate the reactivity of AZ91, hydrolysis, anodic polarization and EIS must be considered.

Keywords: Ball milling; AZ91; $Mg_{17}Al_{12}$; Corrosion; Hydrogen; Electrochemical impedance spectroscopy.

1. Introduction

The way we use fossil fuels as our main source of energy since the industrial revolution has caused a massive increase in the levels of CO_2 and other greenhouse gases in our atmosphere, which is the main cause of global warming [1]. Decarbonizing the energy supply using clean, sustainable and renewable alternative energies is essential for future energy sustainability, global security and climate change [2–7]. Renewable energy resources will play a key role in the transition to a clean and sustainable energy system [8,9]. In fact, hydrogen as an energy carrier is among the most promising solutions to the problems mentioned above [1,10–12].

Hydrogen can be produced using diverse domestic resources, including nuclear, natural gas, coal, biomass, and other renewable sources [13]. The latter include solar, wind, hydroelectric, or geothermal energy. The production of hydrogen can be achieved via various process technologies, namely electrolysis, photolysis, biolysis, thermolysis, plasma arc decomposition of methane, coal gasification, fermentation, etc. [1,9,13–15]. Nowadays, hydrogen is mainly produced by steam reforming of natural gas, a process that leads to massive emissions of greenhouse gases [16,17]. However, all these production techniques are limited for economic, environmental reasons and dependence on resources (especially for production from biomass).

Conversely, hydrogen production by the hydrolysis reaction of magnesium can occur spontaneously under normal conditions of temperature and pressure without any catalyst.

* Corresponding author.
E-mail address: jean-louis.bobet@icmcb.cnrs.fr (J.L. Bobet).

https://doi.org/10.1016/j.jma.2020.12.007

Please cite this article as: S. Al Bacha, I. Aubert, M. Zakhour et al., Valorization of AZ91 by the hydrolysis reaction for hydrogen production (Electrochemical approach), Journal of Magnesium and Alloys, https://doi.org/10.1016/j.jma.2020.12.007

However, magnesium hydrolysis is rapidly interrupted by the formation of a passivation layer of solid magnesium hydroxide on the surface of Mg, which limits the hydrolysis by blocking the diffusion of H_2O to Mg matrix. Recently, many highly reactive Mg-based materials have been developed to improve the hydrogen production by the hydrolysis reaction (*e.g.* Mg_2Si [18], Mg-Mg_2X (X = Cu, Sn) [19], Mg-Ni-Ce [20], $MgNdNi_{15}$ [21], Mg-Mg_2Si [22] Mg – Graphite composites elaborated by plasma-assisted milling [23]) and have been reviewed elsewhere [24]. On the other hand, it has been demonstrated that the hydrolysis of magnesium can be replaced by that of Mg-based alloys and waste [25–33]. This can enable the low-cost production of pure hydrogen by the hydrolysis reaction. On the other hand, ball milling has been shown to be beneficial in improving the reactivity of Mg-based materials. Several milling strategies were investigated such as using various additives, changing the milling atmosphere, varying the rotational speed, using different milling devices [25–38]. In this work, we present the production of hydrogen by the hydrolysis reaction of an AZ91 alloy. This "standard" alloy has schematically an Mg matrix and an $Mg_{17}Al_{12}$ intermetallic phase [39–41].

Previously [35], we showed that ball milling for 5 h at 250 rpm under inert atmosphere (*i.e.* Ar) enhances the hydrolysis reaction performance of $Mg_{17}Al_{12}$ (from 6% to 11% of the theoretical hydrogen production capacity in 60 min). Upon all the tested additives (*i.e.* graphite, NaCl, $MgCl_2$ and $AlCl_3$), $AlCl_3$ showed the best performance due to the beneficial effect of its exothermic dissolution. The addition of graphite and $AlCl_3$ simultaneously during ball milling of $Mg_{17}Al_{12}$ further enhances its hydrolysis with a yield of 16% reached in less than 5 min.

In our prior works [32,33], Mg alloys waste (AZ31 mixed with Al scraps in a proportion closer to that existing in AZ91) provided from the sacrificial anode industry was ball milled to enhance its hydrolysis reactivity. Milling under H_2 was found to be less efficient than that under Ar. When using a single additive (*i.e.* graphite or $AlCl_3$), the best hydrolysis properties are obtained with graphite (yield of 95% of its theoretical capacity reached in 5 min) due to the formation of the protective graphite layer. By incorporating both additives sequentially, the best material from the hydrogen production point of view was obtained by milling Mg alloy with G for 2 h and with $AlCl_3$ for 2 extra hours (complete hydrolysis reached in 5 min).

In this present investigation, a "standard" AZ91 (*i.e.* in which Al forms with Mg the intermetallic $Mg_{17}Al_{12}$) is ball milled under Ar using the same mill device following two strategies: The first was used to enhance the hydrolysis performance of $Mg_{17}Al_{12}$ [35] and the second was applied to improve the reactivity of Mg alloy waste [33]. The comparison between both strategies was done by reproducing the best "additive + milling duration" combination on the present AZ91. Hydrogen production by AZ91 is an electrochemical reaction where Mg is oxidized to Mg^{2+} and water is reduced to produce H_2 gas [28]. Thus, the higher hydrolysis performance of Mg-based materials corresponds to higher oxidation of magnesium. As a consequence, both anodic polarization (corresponding to the oxidation of Mg) and hydrolysis tests estimate the reactivity of the powder from an electrochemical and chemical aspects respectively. Hydrolysis test, anodic polarization and electrochemical impedance spectroscopy are used to evaluate the corrosion rate of the milled materials and to investigate the effect of milling strategy on the hydrolysis properties of the materials [42].

Table 1
Milling conditions used in each strategy.

Parameter	$Mg_{17}Al_{12}$ study conditions [35]	AZ91 study conditions [33]
Rotational speed	250 rpm	350 rpm
Powder-to-ball mass ratio	1/17	1/40
Mill gas	Ar	Ar
Continuous milling	15 min	10 min
Pause	2 min	20 min
Nomenclature	250 rpm	350 rpm

2. Experimental details

2.1. Ball milling

The plate of AZ91 (from a local supplier in Pessac, France) was crushed by face milling to reduce it into pellets. AZ91 milling was performed under Ar at room temperature in a Fritsch Pulverisette 7 planetary mill. The milling strategies used in this work will be named according to the rotational speed. The milling conditions for both strategies are summarized in Table 1.

Based on our previous studies [25,32–35], we have adopted the addition of 5 wt.% of additives (*i.e.* graphite G (Aldrich) and anhydrous aluminum chloride powder $AlCl_3$ (98.5%, Acros Organics)) during ball milling. The powder obtained after ball milling was passed through a sieve of 200 µm and was stored in Argon-filled glove box to avoid air exposure.

2.2. Materials characterization

The structural and morphological properties of AZ91 alloy and milled AZ91 are investigated by X-ray diffraction (Philips PANalyticalX'Pert (PW1820) diffractometer with Cu Kα1 radiation (λ = 1.5405 Å)), scanning electron microscope (TESCAN VEGA3 SB microscope) equipped with energy dispersive X-ray spectrometer (EDS) and laser granulometry in absolute ethanol (MASTERSIZER2000 from Malvern®). Particles size data are expressed as number distribution where d_{90} corresponds to the point in the size distribution, up to and including which, 90% of the total number of particles in the sample is contained.

2.3. Hydrogen production and electrochemical measurements

The hydrolysis reaction was carried out in a "model seawater" solution (*i.e.* 3.5 wt.% NaCl) at room temperature (the experimental setup is detailed in reference [43]). Hydrogen

production is presented as the conversion yield (%), which is defined as the volume of produced hydrogen over the theoretical volume of hydrogen if AZ91 ($Mg + Mg_{17}Al_{12}$) powder is completely consumed.

Open circuit potential (OCP), anodic polarization curve and electrochemical impedance spectrum (EIS) were determined using an electrochemical workstation (Ametek VersaSTAT 3F type) at room temperature in 3.5 wt.% NaCl solution with a classical three-electrode cell setup (described in Ref. [21]). The working electrode was a pellet of 0.80 cm^2 ± 0.05 cm^2 (measured using ImageJ software) and was wet ground with ethanol to a 4000-grit finish before each test. The preparation of the working electrode and the details about the electrochemical tests conditions were performed following the procedure reported in references [21,42]. EIS measurements were carried out over a frequency ranging from 100 kHz to 700 mHz with a 10 mV amplitude sinusoidal voltage at OCP. The EIS results were fitted using the commercial ZView 3.5f software. All above electrochemical measurements were repeated at least twice to ensure reproducibility.

Throughout this work, the materials will be named as follows:

- AZ91 mh: AZ91 milled for m hours
- AZ91 +X mh: AZ91 milled with 5 wt.% of X for m hours
- AZ91 + (X+Y) mh: AZ91 milled with 5 wt.% of X and 5 wt.% of Y for m hours and
- AZ91 + X mh + Y nh: AZ91 milled with 5 wt.% of X for m hours followed by a milling with 5 wt.% of Y for n hours, (X,Y = $AlCl_3$, G).

3. Results

3.1. AZ91 cast alloy

AZ91, consisting mainly of 90 wt.% Mg, 9 wt.% Al and 1 wt.% Zn, is a part of AZ family used in the field of transportation, agriculture, chemical, construction and energy industries owing to its impressive efficient properties such as castability, weldabilty, good machinability, rigidity, toughness and lightness [44–46].

Fig. 1.a shows the X-ray diffraction (XRD) patterns of the AZ91 used in this work. The difference plot of the experimental XRD patterns of AZ91 alloy (open circles) and the calculated XRD patterns of Mg (red line) allows highlighting the presence of the intermetallic $Mg_{17}Al_{12}$. In addition, the difference curve shows that the peaks of Mg are doubled. This is indicative of the existence of a solid solution of Zn into Mg ($Mg_{0.97}Zn_{0.03}$ [47]). Indeed, the substitution of Mg atoms by Zn atoms in the hexagonal crystal lattice of Mg decreases the cell parameters by 0.6% (*a* decreases from 3.21 Å to 3.19 Å and *c* decreases from 5.21 Å to 5.18 Å). In fact, Zn metallic radius (r_{Zn} = 134 pm) is smaller than the one of Mg (r_{Mg} = 160 pm). This results in a slight displacement of the peaks of Mg towards higher 2θ angles (*e.g.* peak of the plane (101) of Mg at 36.62° while that of $Mg_{0.97}Zn_{0.03}$ is at 36.85°). Since the alloy contains 1 wt.% of Zn, the contribution of $Mg_{0.97}Zn_{0.03}$ in the hydrogen production / corrosion behavior of the alloys is considered similar to that of Mg.

Table 2
Mg crystallite size (τ_{Mg}) and particles size d_{90} of all the materials involved in this study.

Sample	Milling speed (rpm)	τ_{Mg} (nm)	Particles size d_{90} (µm)
AZ91	–	23	>300
AZ91 5h	250	24	33
AZ91 + G 5h	250	23	16
AZ91 + $AlCl_3$ 5h	250	22	9
AZ91 + (G + $AlCl_3$) 5h	250	21	6
AZ91 2h	350	22	20
AZ91 + G 5h	350	19	18
AZ91 + $AlCl_3$ 2h	350	20	12
AZ91 + G 2h + $AlCl_3$ 2h	350	17	9

3.2. Ball milling at 250 rpm

In our previous work [35], we stated that cheap additives (*e.g.* Graphite and $AlCl_3$) can be used to improve the hydrolysis of $Mg_{17}Al_{12}$. In this section, we present the effect of ball milling at 250 rpm for 5 h without additives (named AZ91 5 h), with 5 wt.% G (named AZ91 + G 5 h), with 5 wt.% $AlCl_3$ (named AZ91 + $AlCl_3$ 5 h) and with 5 wt.% G and 5 wt.% $AlCl_3$ (named AZ91 + (G+ $AlCl_3$) 5 h).

3.2.1. Structural and morphological modifications

Fig. 1.b shows the X-ray diffractograms of AZ91 alloys milled at 250 rpm before hydrolysis and AZ91 + (G + $AlCl_3$) 5 h after hydrolysis. The slight variation of the width of the diffraction peaks indicates an insignificant variation in the size of Mg crystallites (τ_{Mg} of approximately 23 nm, *Cf* Table 2). Nevertheless, mechanical milling reduces the particles size from more than 300 µm for unmilled AZ91 to 6 µm for AZ91 + (G + $AlCl_3$) 5 h (Table 2). These observations indicate that the milling at 250 rpm is not energetic enough to decrease Mg crystallite size. The reduction in particles size, on the other hand, is probably due to the effect of ball milling additives.

Indeed, the milling of AZ91 for 5 h without additives reduces the particles size to 33 µm (Fig. 2.a and Table 2) while milling with 5 wt.% of graphite for 5 h decreases the particles size to 16 µm (Fig. 2.b and Table 2). Milling with $AlCl_3$ (*i.e.* AZ91 + $AlCl_3$ 5 h) and with both graphite and $AlCl_3$ (*i.e.* AZ91 + (G + $AlCl_3$) 5 h) further reduces the particles size and creates surface defects (Fig. 2.c and d and Table 2). The beneficial effect of ball milling of Mg and $Mg_{17}Al_{12}$ (*i.e.* the main components of the AZ91 alloy) with both additives has been reported in the literature [34,35,37]. Indeed, graphite forms a protective layer on the surface of Mg [34,37] and $Mg_{17}Al_{12}$ [35] while the addition of $AlCl_3$ reduces the particles size and favors the formation of surface defects (*e.g.* cracks).

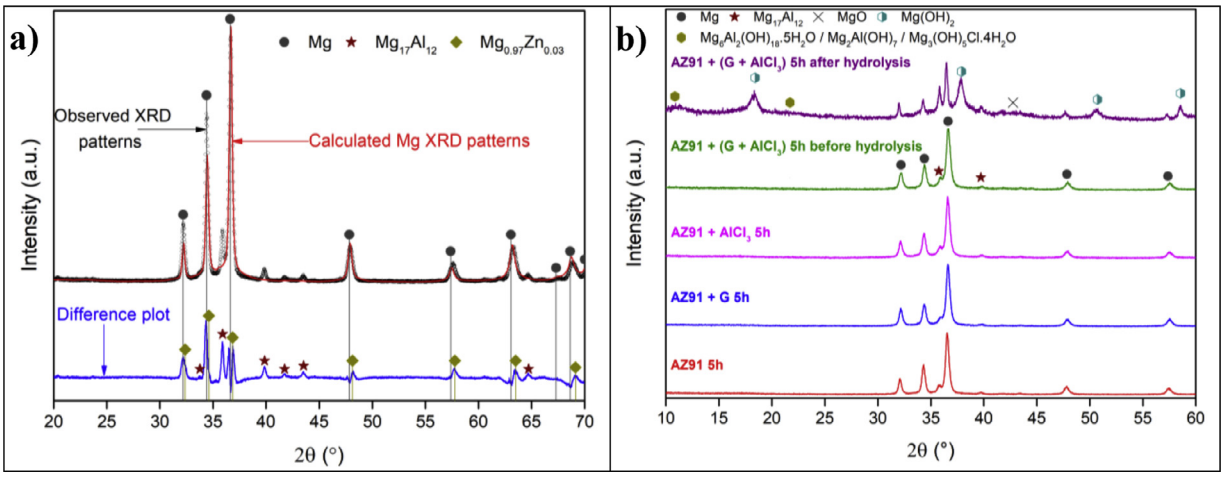

Fig. 1. a) Observed (open circles) and calculated (red line) X-ray diffraction patterns of AZ91 with the difference (blue line) at the same scale plotted below and b) XRD patterns of AZ91 5 h, AZ91 + G 5 h, AZ91 + $AlCl_3$ 5 h and AZ91 + (G + $AlCl_3$) 5 h milled at 250 rpm before hydrolysis and AZ91 + (G + $AlCl_3$) 5 h after hydrolysis.

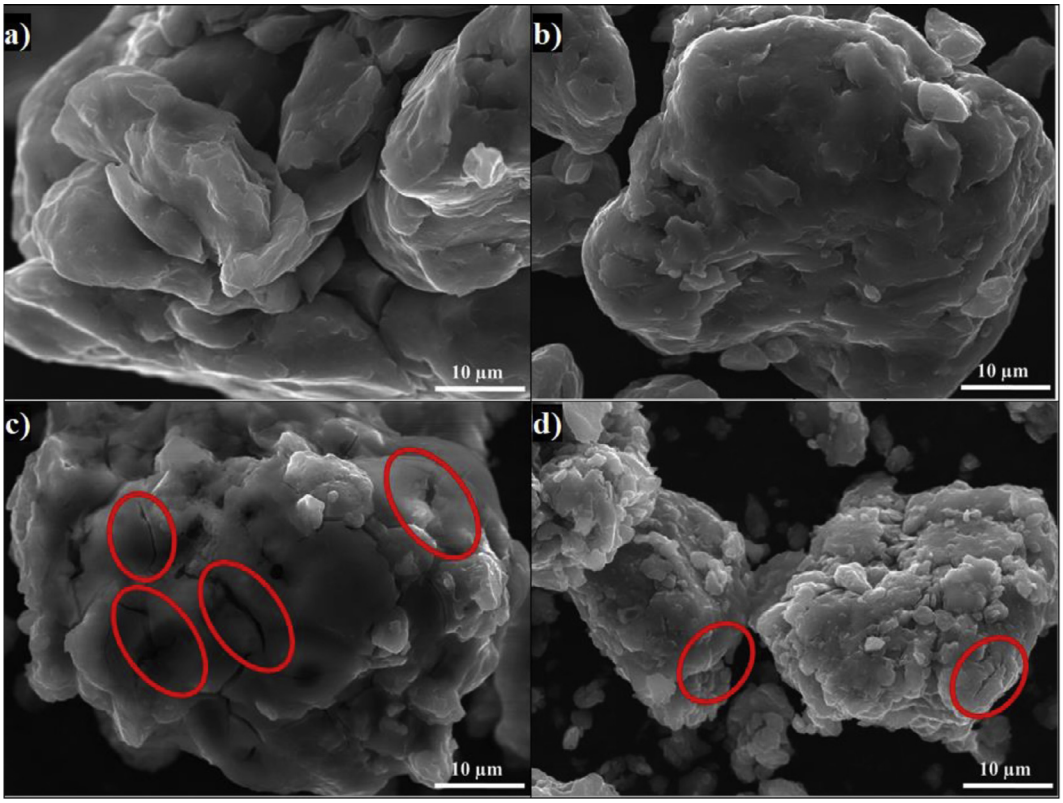

Fig. 2. SEM images of a) AZ91 5 h, b) AZ91 + G 5 h, c) AZ91 + $AlCl_3$ 5 h and d) AZ91 + (G + $AlCl_3$) 5 h milled at 250 rpm. Red circles indicate surface defects formed during ball milling with $AlCl_3$.

3.2.2. Hydrogen production

Fig. 3.a and b show the hydrogen production evolution by the hydrolysis of the milled AZ91 at 250 and 350 rpm, respectively. AZ91 flakes barely react with NaCl solution with only a production of 7% of its theoretical production capacity in 60 min of reaction. Note that the theoretical production capacity was calculated for each sample taking into account the equations for the hydrolysis of Mg and $Mg_{17}Al_{12}$ [35] and the composition of the milled material (*i.e.* quantification of the 2 phases) evaluated from XRD refinements (78 wt.% of Mg and 21 wt.% of $Mg_{17}Al_{12}$).

Milling AZ91 for 5 h at 250 rpm improves hydrolysis performance with a production of 20% of the theoretical H_2 generation capacity in 60 min while milling with graphite for the same duration (*i.e.* AZ91+ G 5 h) increases the production of hydrogen to 50% (Fig. 3.a). This can be ex-

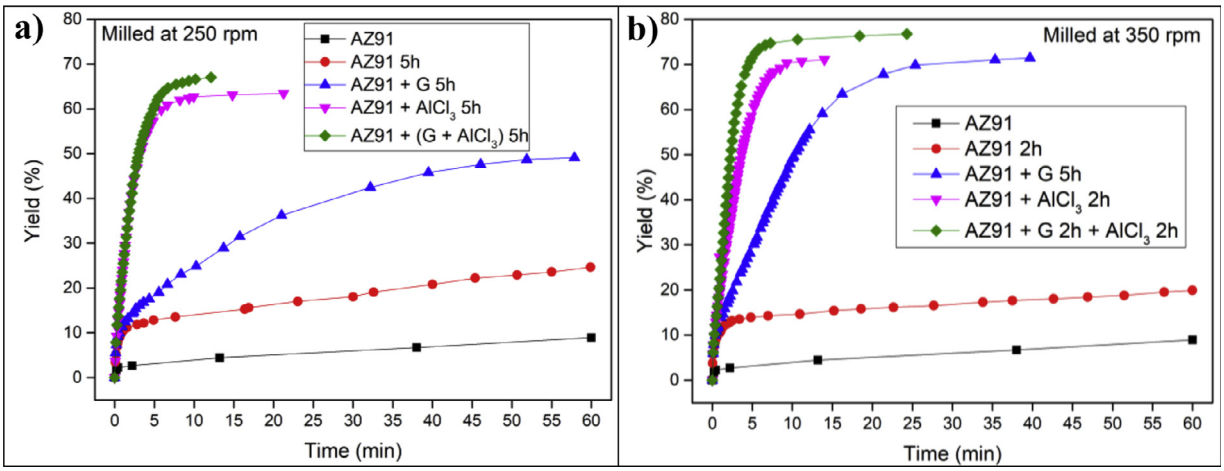

Fig. 3. Hydrogen generation of a) AZ91, AZ91 5 h, AZ91 + G 5 h, AZ91 + $AlCl_3$ 5 h and AZ91 + (G + $AlCl_3$) 5 h milled at 250 rpm and b) AZ91, AZ91 2 h, AZ91 + G 5 h, AZ91 + $AlCl_3$ 2 h and AZ91 + G 2 h + $AlCl_3$ 2 h milled at 350 rpm.

plained by the formation of the protective layer of graphite [25,34] which prevents the adhesion of the passive $Mg(OH)_2$ on the surface. However, the best performances were obtained for AZ91 + $AlCl_3$ 5 h and AZ91 + (G + $AlCl_3$) 5 h with a production of 65% of the theoretical capacity in approximately 25 min and 10 min of reaction respectively. The exothermic dissolution of $AlCl_3$ during the hydrolysis of AZ91 milled with $AlCl_3$ generates, at the material-solution interface, H^+ and Al^{3+} acidic ions which promotes the dissolution of $Mg(OH)_2$ [35,48–50]. Previously, we have shown that ball milling improves the hydrolysis of $Mg_{17}Al_{12}$ and the reactivity was reported as follow: $Mg_{17}Al_{12}$ < $Mg_{17}Al_{12}$ + G 5 h < $Mg_{17}Al_{12}$ 5 h < $Mg_{17}Al_{12}$ + $AlCl_3$ 5 h < $Mg_{17}Al_{12}$ + G + $AlCl_3$ 5 h [35]. As expected, the reactivity of ball milled AZ91 varies in the same way as that of $Mg_{17}Al_{12}$ with a dissimilarity when milling with graphite which enhances the hydrolysis performance more than AZ91 5 h. These results highlight that contribution of $Mg_{17}Al_{12}$ plays a key role in the overall hydrolysis reaction of AZ alloys. When AZ91 is milled with an additive, this latter will affect the reactivity of both Mg and $Mg_{17}Al_{12}$. $AlCl_3$ enhances the hydrolysis performance of Mg [48,49] and $Mg_{17}Al_{12}$ [35] while graphite only improves the hydrolysis performance of Mg [34] (no significant improvement was observed for $Mg_{17}Al_{12}$ [35]).

XRD patterns of AZ91 + (G + $AlCl_3$) 5 h after the hydrolysis (Fig. 1.b) reveal the presence of Mg peaks which confirm the incomplete reaction between AZ91 and the aqueous solution. Moreover, the formation of $Mg_xAl_y(OH)_z$ phases confirms that the milling strategy increases the hydrolysis reactivity of $Mg_{17}Al_{12}$ since a part of Al (from $Mg_{17}Al_{12}$) contributes in the hydrogen production while the XRD patterns of AZ91 5 h and AZ91 + G 5 h after the hydrolysis (*Cf* Supplementary material Fig. 1) reveals the presence of Mg, $Mg_{17}Al_{12}$ and $Mg(OH)_2$ but no $Mg_xAl_y(OH)_z$ can be detected.

Open circuit potential (implying the corrosion potential E_{corr}) for all the materials were recorded during 30 min of immersion in 3.5 wt.% NaCl aqueous solution. The corrosion

Table 3
OCP values and corrosion current density (J_{corr}) for all the materials involved in this study.

Sample	Milling speed (rpm)	OCP (V/SCE)	J_{corr} (mA/cm^2)
AZ91	–	−1.63±0.05	0.03±0.001
AZ91 5h	250	−1.55±0.04	4.1±0.2
AZ91 + G 5h	250	−1.51±0.04	0.7±0.05
AZ91 + $AlCl_3$ 5h	250	−1.52±0.04	4.8±0.8
AZ91 + (G + $AlCl_3$) 5h	250	−1.50±0.04	7.5±0.3
AZ91 2h	350	−1.54±0.04	4.9±0.2
AZ91 + G 5h	350	−1.51±0.04	8.3±0.4
AZ91 + $AlCl_3$ 2h	350	−1.53±0.04	10.4±0.4
AZ91 + G 2h + $AlCl_3$ 2h	350	−1.50±0.04	11.3±0.4

potentials E_{corr} presented in Table 3 were obtained by averaging OCP values from 15 min to 30 min where the potential was the most stable. AZ91 alloy has an E_{corr} of -1.63 V/SCE (Table 3) while Singh *et al.* [51] reported an OCP of -1.5 V/SCE. In fact, galvanic coupling exists between Mg and $Mg_{17}Al_{12}$ [21,42]. Mechanical and thermal treatments during the manufacture of Mg-Al alloys affect the precipitation of the intermetallic in Mg so that the distribution of $Mg_{17}Al_{12}$ in the matrix varies [52]. This affects the surface area between each phase as well as the OCP [53]. Ball milling at 250 rpm for 5 h shifts the OCP toward higher potentials (E_{corr} = -1.55 V/SCE). The increase in E_{corr} for milled AZ91 indicates a higher reactivity to form the passivation layer $Mg(OH)_2$ [54]. The variation of the OCP of AZ91 + G is attributed to the galvanic coupling established between Mg-G and $Mg_{17}Al_{12}$-G

The corrosion current densities (J_{corr}) are determined from the anodic polarization curves [55]. The anodic polarization curve (Fig. 4.a) demonstrates the formation of a passivation film for AZ91, while the passivation is negligible when the alloy is milled with and without additives. AZ91 corrodes in the "model" seawater solution with a corrosion current density of 0.03 mA/cm^2 (Table 3) in total agreement with that reported previously (J_{corr} = 0.0255 mA/cm^2 according to ref. [51]). As

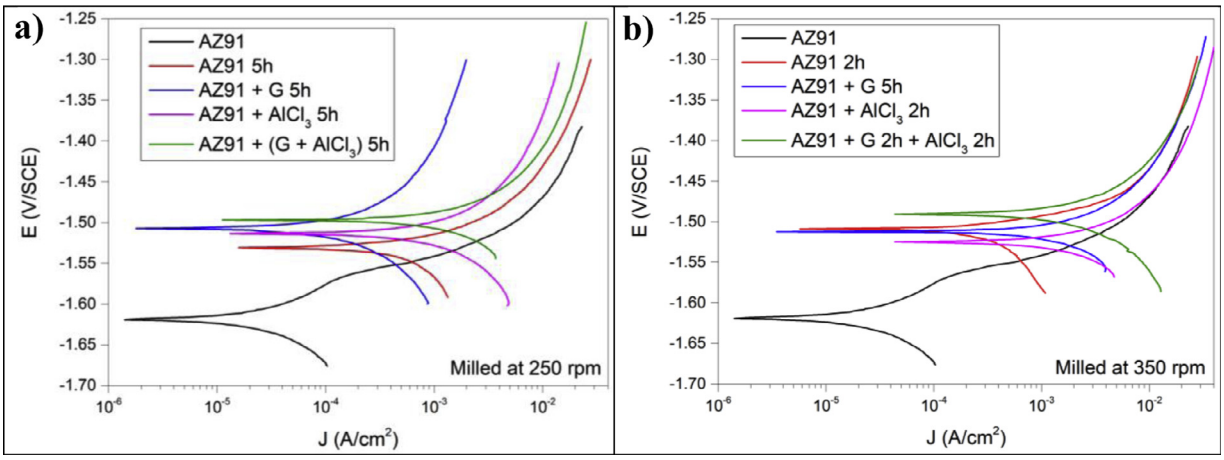

Fig. 4. Anodic polarization curves for a) AZ91, AZ91 5 h, AZ91 + G 5 h, AZ91 + $AlCl_3$ 5 h and AZ91 + (G + $AlCl_3$) 5 h milled at 250 rpm and b) AZ91, AZ91 2 h, AZ91 + G 5 h, AZ91 + $AlCl_3$ 2 h and AZ91 + G 2 h + $AlCl_3$ 2 h milled at 350 rpm in 3.5 wt.% NaCl aqueous solution.

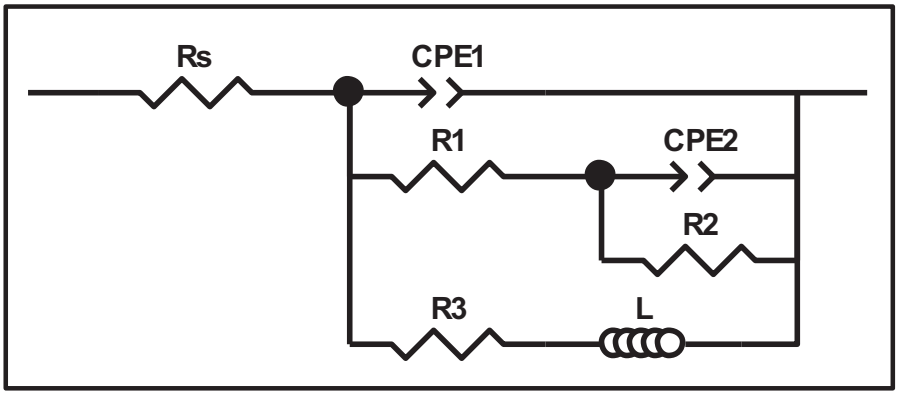

Fig. 5. Electrical equivalent circuit used to interpret the experimental impedance data.

evaluated by the hydrolysis tests, ball milling increases the corrosion rate of the milled materials to 4.1 mA/cm^2 for AZ91 5 h and a maximum reactivity for AZ91 + (G + $AlCl_3$) 5 h with J_{corr} = 7.5 mA/cm^2 (Table 3).

On the other hand, a dissimilarity between the hydrolysis test and anodic polarization is observed for AZ91 + G 5h: The hydrolysis test shows that AZ91 + G 5 h is more reactive than AZ91 5 h while the anodic polarization test shows that AZ91 5 h is more reactive. Such dissimilarity is due to the presence of the protective graphite layer on the surface of the pellets during the polarization test which changes the electrical properties of the surface.

3.2.3. Electrochemical impedance spectroscopy

EIS is known as an efficient method to investigate the effect of ball milling additives on the corrosion behavior of materials [34]. Therefore, we investigate the electrical properties of the milled materials surface during immersion in NaCl solution by electrochemical impedance spectroscopy measurements. The Nyquist EIS spectra of AZ91 and milled AZ91 at OCP display a capacitive loop ($Z_{im} < 0$) and an inductive loop ($Z_{im} > 0$, *Cf* Fig. 5). Previously, Cao *et al.* [56] fitted the EIS experimental data of AZ91 by neglecting the presence of the inductive loop. King *et al.* [57] considered the contribution of the inductive loop (by adding an inductor to their electrical equivalent circuit) while fitting the EIS data of pure Mg in NaCl solution. The inductive loop can be interpreted by the formation of a reaction intermediate (*i.e.* multi-step reaction) [55,58–60] and its adsorption on the surface. It is worth noting that the inductive loop is not a measurement artefact.

In the present study, we adopted the equivalent circuit of King *et al.* [57] to fit our experimental data and we used constant phase element (CPE) for the representation of the capacitive elements (Fig. 5).

Fig. 6 shows relevant examples of the various impedance curves obtained for AZ91 and AZ91 milled at 250 rpm. EIS spectra of AZ91 + G 5 h and AZ91 + (G + $AlCl_3$) 5 h (Supplementary material Fig. 2.a and b, respectively) are similar to AZ91 + $AlCl_3$ 5 h (Fig. 6.c). The effective capacitances for both CPE1 and CPE2 were calculated from the values of the capacitance Q(i), the CPE exponent order n(i) and the associated resistance R(i) [61]. For CPE1, n1 values are greater than 0.5 while for CPE2, n2 decreases to 0.55 in the case of AZ91 + (G + $AlCl_3$) 5 h indicating that the corrosion mechanism becomes diffusional. The values of all electrochemical parameters of AZ91 and milled AZ91 at 250 rpm determined

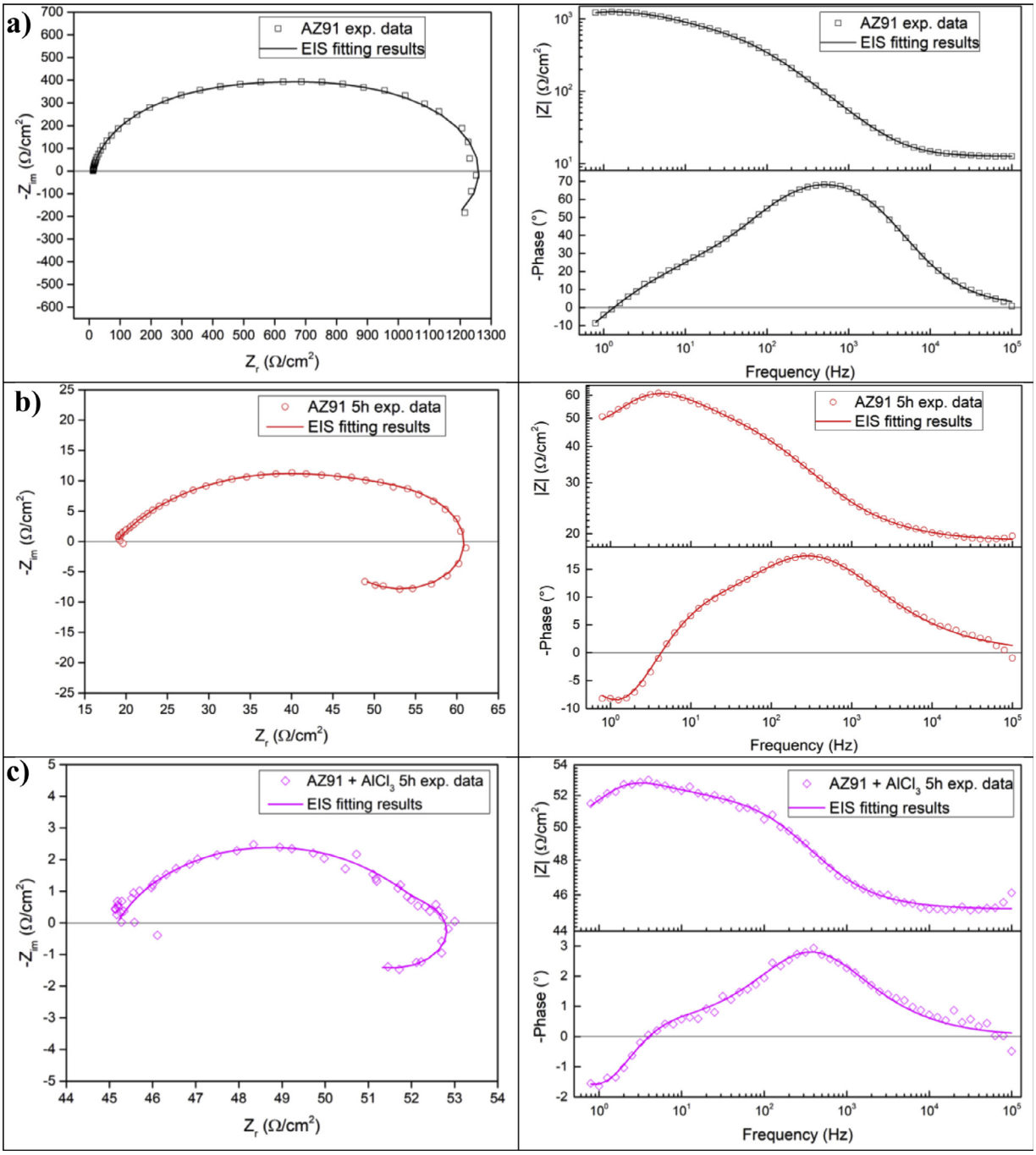

Fig. 6. Nyquist (left) and Bode (right) plots for: a) AZ91, b) AZ91 5 h, and c) AZ91 + $AlCl_3$ 5 h milled at 250 rpm.

using ZView software are summarized in Supplementary material Table 1.

From the EIS fitting results, equivalent circuit parameters were calculated and presented in Table 4. R_s is the solution resistance, C_1 and C_2 are the effective capacitances of CPE1 and CPE2 respectively, R_t the charge transfer resistance and R_p the polarization resistance. Based on the calculated values of the capacitances, C_1 is most likely a double layer capacitance on a roughened electrode [57,62,63] while C_2 characterizes the pseudo capacitance of the adsorption of a corrosion intermediate (*e.g.* Mg^+ [55,59,60,64] or MgH^+ [58]) or a corrosion product (*i.e.* $Mg(OH)_2$). High C_2 values were justified and discussed for pseudo capacitance in previous investigations [57,65] and the variation in the capacitance is proportional to the surface of the working electrode. Ball milling for 5 h at 250 rpm reduces the particles size of AZ91 to 33 µm (Table 2). Note that electrochemical tests are performed using condensed powder. Consequently, milled AZ91 electrode shows more grain boundaries than unmilled AZ91 which act as reaction (*i.e.* corrosion and hydrolysis) initiator sites and increase the reaction kinetics. Moreover, when corrosion rate increases, the surface of the pellets (*i.e.* working

Table 4
Electrochemical parameters calculated from best fit of impedance data of AZ91, AZ91 5h, AZ91 + G 5h, AZ91 + $AlCl_3$ 5h and AZ91 + (G + $AlCl_3$) 5h milled at 250rpm.

	AZ91	AZ91 5h	AZ91 + G 5h	AZ91 + $AlCl_3$ 5h	AZ91 + (G + $AlCl_3$) 5h
R_s (Ω/cm^2)	13	19	26	45	16
n1	0.92	0.64	0.9	0.75	1
C_1 ($\mu F/cm^2$)	5	47	181	240	140
n2	0.67	0.9	0.67	0.89	0.55
C_2 ($\mu F/cm^2$)	9	∞	∞	∞	∞
R_t (Ω/cm^2)	1245	42	16	8	11
R_p (Ω/cm^2)	700	27	13	5	8

electrode) becomes rougher (consequently the surface area increases) due to the formation of soluble $MgCl_2$ in NaCl solution [21]. C_1 increases from 5 $\mu F/cm^2$ for AZ91 to 47 $\mu F/cm^2$ for AZ91 5h and higher than 100 $\mu F/cm^2$ for AZ91 milled with additives (Table 4). This variation is expected since the capacitance is proportional to the surface area of the working electrode (*i.e.* AZ91 pellets).

The charge transfer resistance R_t is determined from the EIS Nyquist plot where $Z_{im} \rightarrow 0\,\Omega/cm^2$ (at $f > 0$ Hz) and the polarization resistance R_p is estimated by $\frac{1}{Rp} = \frac{1}{R1+R2} + \frac{1}{R3}$ (where $Z_{im} \rightarrow 0\ \Omega/cm^2$ at $f \rightarrow 0$ Hz) [57]. For both resistances, the rise in their value is attributed to lower corrosion resistance. In the literature, R_t is considered when evaluating the corrosion rate by EIS without considering the inductive loop. Hence, the corrosion rate is underestimated by a factor of 2 [57]. Table 4 shows that R_t is higher than R_p as stated by King *et al.* [57] due to the contribution of the inductive loop (by the resistance R_3) in the calculation of the polarization resistance. R_p decreases from 700 Ω/cm^2 for AZ91 to 27 Ω/cm^2 after ball milling mainly for the reason that R_p is inversely proportional to the surface area (while the surface area varies and the corrosion rate vary proportionally previously indicated) [61]. The calculated R_p for milled AZ91 shows that AZ91 + G 5h is less corrosion resistant than AZ91 5h as stated by the hydrolysis test. This dissimilarity between J_{corr} determined by anodic polarization technic and R_p is probably attributed to the protective graphite layer as previously mentioned. The increase of C_1 values and the diminution of R_p and R_t for milled AZ91 is attributed to the destabilization of $Mg(OH)_2$ induced by the presence of additives. In fact, the exothermic dissolution of $AlCl_3$ during the immersion of AZ91 + $AlCl_3$ 5h in NaCl solution increase the temperature at the interface material-solution and generates locally Lewis acid cations Al^{3+}et Brønsted acid cations H^+ [48,54] which increase the solubility of $Mg(OH)_2$ at the interface. While the presence of graphite during the mechanical treatment forms a protective layer which prevents the adhesion of $Mg(OH)_2$ on the surface.

The inclusion of inductor was justified in previous reports [57,63] and is attributed to the adsorption of corrosion intermediate (*e.g.* Mg^+ [55,59,60,64] or MgH^+ [58]). However, the inductance values (L) shown in Supplementary materials Table 1 are only considered as qualitative indication of the formation of reaction intermediate.

3.3. Ball milling at 350rpm

Ball milling of Mg alloy used in sacrificial anode industry at high speed under H_2 [32] and under Ar [33] ameliorates its hydrolysis performance. We showed that milling under H_2 is less efficient than that under Ar, in term of hydrolysis performances, due to the formation of less reactive MgH_2 [32]. Extending milling time to more than 2h without additives or with $AlCl_3$ deteriorated the hydrolysis performance while Mg alloy milled with graphite for 5h was optimal and generates 95% of its total H_2 production capacity in 5 min [33]. The best hydrolysis performance was obtained by milling with graphite for 2h followed by milling for additional 2h with $AlCl_3$. Finally, we showed that milling using the "high-energy" Fristch Pulverisette (the same mill device used in this investigation) was more beneficial than the "low-energy" Australian Uni-Ball-II.

Higher milling speed was proved beneficial to ameliorate the hydrolysis reactivity of Mg-based alloy, so that AZ91 was milled at 350rpm and the milling time was chosen based on these previous studies. Therefore, AZ91 2h, AZ91 + $AlCl_3$ 2h, AZ91 + G 5h and AZ91 + G 2h + $AlCl_3$ 2h milled at 350rpm were analyzed in this work. The structural and morphological properties and the hydrogen production performances (*i.e.* hydrolysis, anodic polarization and EIS) of AZ91 2h, AZ91 + $AlCl_3$ 2h, AZ91 + G 5h and AZ91 + G 2h + $AlCl_3$ 2h milled at 350rpm are reported below.

3.3.1. Structural and morphological modifications

Milling AZ91 at higher energy (i.e. 350rpm) decreases Mg crystallite size from 22 to 17nm and particles size from 20 to 9 μm for AZ91 2h and AZ91 + G 2h + $AlCl_3$ 2h respectively (*Cf* XRD patterns are shown in Supplementary material figure 3). Milling with $AlCl_3$ further decreases particles size to 12 μm for AZ91 + $AlCl_3$ 2h. In fact, chlorides are known as excellent milling agents because they improve the efficiency of the milling process by creating microstructural defects and enabling the reduction of particles size thus increasing the surface area [66].

SEM micrographs display particles size reduction after ball milling for 2h (Fig. 7.a), the formation of relative flat surface in AZ91 + G 5h (Fig. 7.b) and microstructural defects (*i.e.* cracks) in AZ91 + $AlCl_3$ 2h (Fig. 7.c). The surface roughness of AZ91 + G 2h + $AlCl_3$ 2h is justified by the effect of

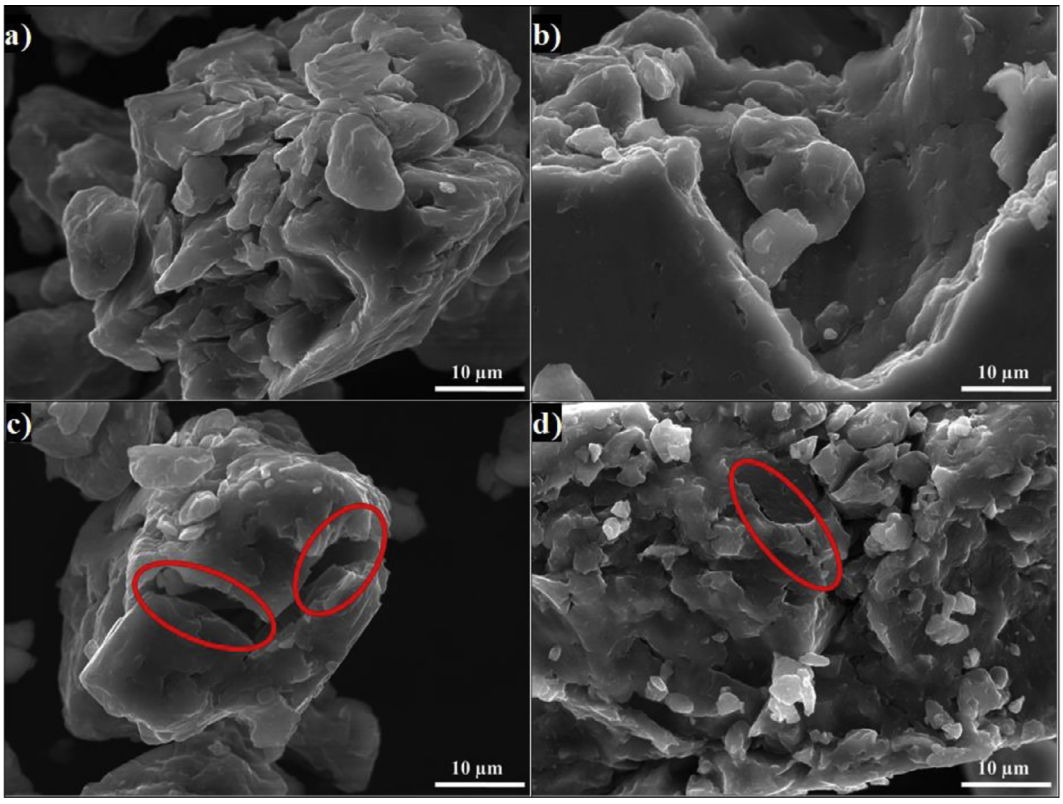

Fig. 7. SEM images of a) AZ91 2 h, b) AZ91 + G 5 h, c) AZ91 + $AlCl_3$ 2 h and d) AZ91 + G 2 h + $AlCl_3$ 2 h milled at 350 rpm. Red circles indicate surface defects formed during ball milling with $AlCl_3$.

both additives (flat surface during the first milling with G and cracks formation when $AlCl_3$ is added, *Cf* Fig. 7.d).

3.3.2. Hydrogen production

Ball milling AZ91 for 2 h at 350 rpm enhances its hydrolysis performance with a production of 15% of the theoretical H_2 volume in 60 min (Fig. 3.b). AZ91 + G 5 h generates 65% of its theoretical generation capacity in 35 min while AZ91 + $AlCl_3$ 2 h produces the same H_2 volume in only 8 min. Fig. 3.b shows that the best hydrolysis performances were obtained for AZ91 + G 2 h + $AlCl_3$ 2 h with 75% of its theoretical H_2 generation capacity reached in less than 5 min. The reactivity, in term of hydrolysis performances, of the AZ91 milled in this study varies in the same order as the milled AZ91 sacrificial anodes [32]. The slightly lower hydrolysis performance obtained with this present AZ91 alloy is attributed to the presence of less corrosive $Mg_{17}Al_{12}$ [35] since only Al (no $Mg_{17}Al_{12}$) was detected in the sacrificial anode AZ91 [33].

Open circuit potential of AZ91 milled at 350 rpm increases from -1.63 V/SCE for un-milled AZ91 to an average of -1.52 V/SCE. This variation is attributed, as mentioned in Section 3.2.2, to the formation of $Mg(OH)_2$ on the surface during the immersion in the "model" seawater solution while the increase of the OCP for AZ91 milled with graphite is attributed to a galvanic coupling between Mg – G and $Mg_{17}Al_{12}$ – G. On the other hand, anodic polarization measurements (Fig. 3.b and last 4 rows of Table 3) confirm the hydrolysis results mentioned above. Indeed, the calculated current density (J_{corr}) increases from 0.03 mA/cm^2 for AZ91 alloy to 4.9 mA/cm^2 for AZ91 2 h, 8.3 mA/cm^2 for AZ91 + G 5 h, 10.4 mA/cm^2 for AZ91 + $AlCl_3$ 2 h and 11.3 mA/cm^2 for AZ91 + G 2 h + $AlCl_3$ 2 h (Table 3). The effect of each milling additive was reported in Section 3.2.

3.3.3. Electrochemical impedance spectroscopy

EIS spectra (Nyquist plot) of AZ91 milled at 350 rpm display the presence of a capacitive and an inductive loop (Fig. 8). AZ91 2 h and AZ91 + $AlCl_3$ 2 h spectra display the same trend as AZ91 + G 5 h and AZ91 + G 2 h + $AlCl_3$ 2 h (Supplementary material Fig. 4). Electrochemical parameters calculated from the fit of the experimental data are represented in Table 5. The electrochemical parameters determined using ZView software are summarized in supplementary material Table 2.

The double layer capacitance C_1 increases to 20 µF/cm^2 for AZ91 2 h and 130 µF/cm^2 for AZ91 + G 5 h (Table 5). The decrease in C_1 for AZ91 milled with $AlCl_3$ may be attributed to the dissolution of $AlCl_3$ which changes the composition of the electrolyte at the interface material-electrolyte. As observed previously (Section 3.2.3), R_t are higher than R_p due to the consideration of the inductive loop in the calculations. Moreover, both R_p and R_t decrease in the following order: AZ91 2 h < AZ91 + G 5 h < AZ91 + $AlCl_3$ 2 h < AZ91 + G 2 h + $AlCl_3$ 2 h.

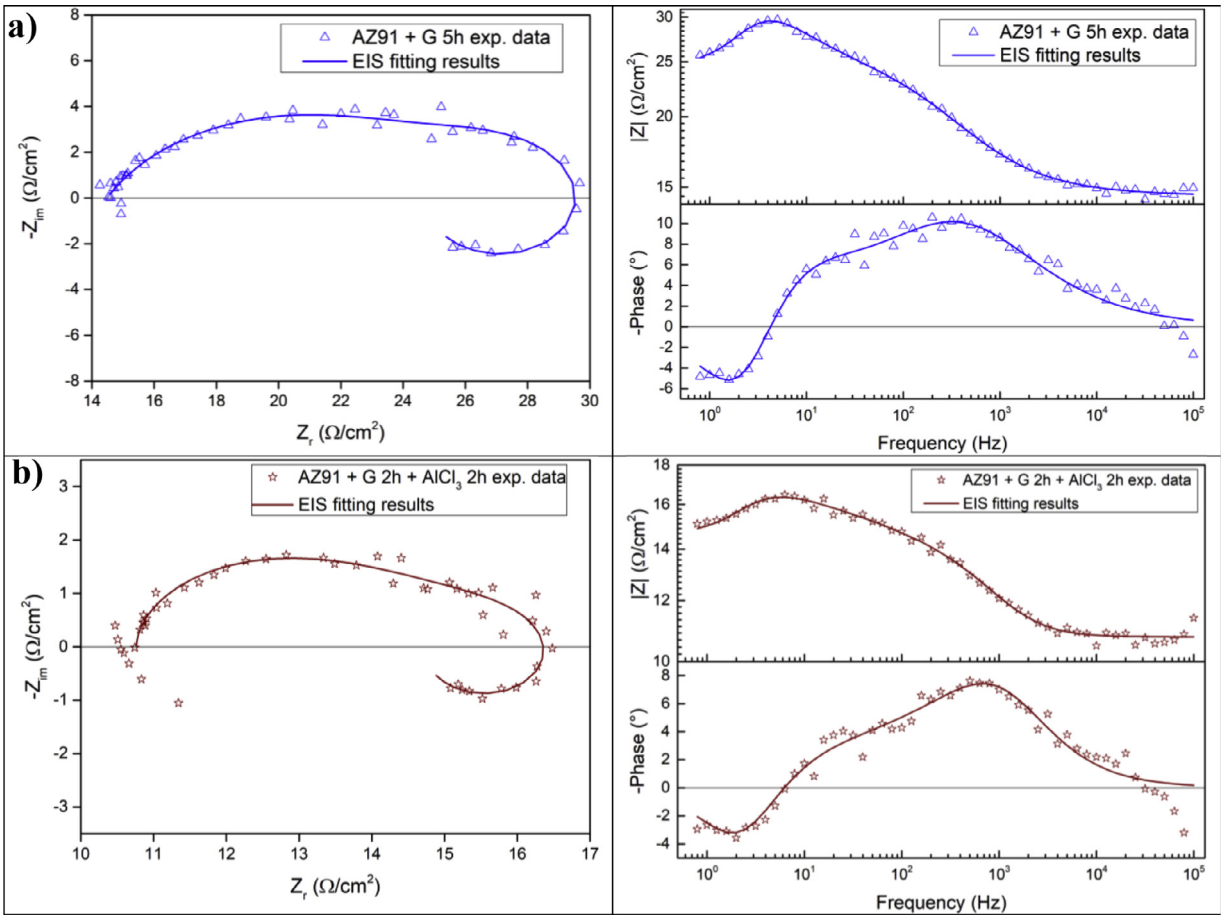

Fig. 8. Nyquist (left) and Bode (right) plots for: a) AZ91 + G 5 h and b) AZ91 + G 2 h + $AlCl_3$ 2 h milled at 350 rpm.

Table 5
Electrochemical parameters calculated from best fit of impedance data of AZ91, AZ91 2 h, AZ91 + G 5 h, AZ91 + $AlCl_3$ 2 h and AZ91 + G 2 h + $AlCl_3$ 2 h milled at 350 rpm.

	AZ91	AZ91 2h	AZ91 + G 5h	AZ91 + $AlCl_3$ 2h	AZ91 + G 2h + $AlCl_3$ 2h
R_s (Ω/cm^2)	13	15	15	10	11
C_1 ($\mu F/cm^2$)	5	20	130	90	80
C_2 ($\mu F/cm^2$)	9	1.3	∞	∞	∞
R_t (Ω/cm^2)	1245	90	15	8	6
R_p (Ω/cm^2)	700	56	10	5	4

EIS results are in accordance with the results obtained by the hydrolysis tests and the anodic polarization measurements. In fact, ball milling with the chronological addition of graphite and $AlCl_3$ is beneficial to improve the reactivity of AZ91 alloy. On the other hand, milling for shorter duration (*e.g.* 2 h) with $AlCl_3$ is better than milling with graphite for 5 h (J_{corr} (AZ91 + $AlCl_3$ 2 h) = 10.4 mA/cm^2 > J_{corr} (AZ91 + G 5 h) = 8.3 mA/cm^2).

4. Comparison between both milling strategies

The crystallinity of AZ91 is affected by the milling strategy: Mg crystallite size is approximately constant for AZ91 milled at 250 rpm while τ_{Mg} decreases more for AZ91 milled at 350 rpm (Table 2). As for particles size d_{90}, milling at 350 rpm without additives further decreases the particles size (33 μm for AZ91 5 h *vs.* 20 μm for AZ91 2 h, *Cf* Table 2). For AZ91 + G 5 h milled at 250 and 350 rpm, the approximately same d_{90} values can be attributed to the lubricant effect of *G* which minimizes the effect of ball-powder collisions.

AZ91 milled at 350 rpm are more reactive with the "model" seawater solution than those milled at 250 rpm. Indeed, AZ91 + G 5 h milled at 350 rpm generates 65% of its theoretical H_2 generation capacity in 35 min while the same material milled at 250 rpm generates only 45% of its theoretical H_2 generation capacity in 60 min. Extending milling time with graphite promotes the homogeneous repartition of graphite on the surface of AZ91 hence forming a "continuous" protective layer. On the other hand, the addition of $AlCl_3$ improves the hydrolysis performance of AZ91 more than

graphite. In fact, $AlCl_3$ enhanced the hydrolysis performance of $Mg_{17}Al_{12}$ [35] which constitutes 21 wt.% of AZ91 alloy. The synergetic effect of G and $AlCl_3$ is beneficial whatever the milling rotation speed. Nevertheless, the chronological addition of G followed by $AlCl_3$ (*i.e.* AZ91 + G 2 h + $AlCl_3$ 2 h) leads to the highest reactivity in term of hydrolysis performances with a generation of 75% of its theoretical capacity in few minutes [32,33].

OCP of milled materials is only affected by the milling additives. For example, each of the following couple of materials have the same potential: AZ91 milled without additives, AZ91 milled with graphite, AZ91 milled with $AlCl_3$ and AZ91 milled with graphite and $AlCl_3$ (Table 3). The corrosion current densities were higher for AZ91 milled at 350 rpm (except for AZ91 milled without additives) in agreement with the hydrolysis tests results.

EIS measurements are an efficient tool to evaluate the effect of milling strategies. In this study, we are interested in evaluating the variation of R_p and R_t since it permits the estimation of the corrosion rate (*i.e.* R_p and R_t are inversely proportional to J_{corr}). The double layer capacitance C_1 is higher for AZ91 milled at 250 rpm suggesting higher thickness of the passivation layer formed on the surface during the immersion in 3.5 wt.% NaCl solution. Conversely, R_t and R_p are lower for AZ91 milled at 350 rpm indicating higher corrosion rate for these materials. Note that AZ91 + G 5 h in both cases (*i.e.* 250 and 350 rpm) reveals approximately the same electrochemical parameters calculated from EIS fitting. Moreover, AZ91 + $AlCl_3$ 2 h and AZ91 + $AlCl_3$ 5 h shows approximately the same R_p and R_t. This suggests that the electrical properties of the surface in combination with physico-chemical processes are only affected by the milling additive and not by the global milling strategy (*i.e.* milling rotational speed, powder to ball mass ratio and milling sequence).

5. Conclusion

In brief, both milling strategies lead to activate a "standard" AZ91 alloy (*i.e.* contains Mg, $Mg_{17}Al_{12}$ and $Mg_{0.97}Zn_{0.03}$) and enhance its hydrolysis performance. However, milling at 350 rpm is more energetic and improves the most the reactivity of AZ91. The best material (yield of 75% reached in less than 5 min) was obtained by chronological addition of G and $AlCl_3$ where AZ91 was milled at 350 rpm for 2 h with graphite followed by further milling for 2 h with $AlCl_3$. By this process, the hydrolysis yield and consequently the corrosion rate increased by more than 400% compared to AZ91 ball milled 2 h at 350 rpm and almost 1000% compared to AZ91 alloy. H_2 production was also faster: this ball milling strategy leads to the multiplication of the hydrogen generation rate by 60 and 128 times compared to AZ91 ball milled 2 h at 350 rpm and AZ91 alloy respectively.

The evaluation of the reactivity of the milled materials is more complex. The rapid Mg dissolution rates complicates the process of determining long-term corrosion rates via anodic polarization. Furthermore, EIS measurements elucidate the effect of the presence of milling additives without distinguishing between 2 materials milled with the same additives but with different strategies. Additionally, the dissimilarity between electrochemical tests and hydrolysis tests can be attributed to the morphological properties of the material. In fact, powders are used for the hydrolysis test while pellets from condensed powder are used in the electrochemical tests. We believe that, in order to investigate the hydrogen production from a material (hence its corrosion), the three technics (*i.e.* hydrolysis, anodic polarization and EIS) should be considered. The corrosion rate estimated by EIS measurements (*i.e.* R_p and R_t) is only relevant on the milling additive effect and not on the milling strategy effect.

To conclude, starting from a "standard" AZ91, one of the most corrosion-resistant Mg-based alloys, we improved the hydrogen production by its hydrolysis in a "model" seawater solution with a generation of 75% in a few minutes. Replacing pure Mg with Mg-based waste will reduce the cost of hydrogen production by this technology. Therefore, by using this "green" hydrogen generator with a proton-exchange membrane fuel cell, a clean energy generator can be established for light and/or short distance mobility.

Declaration of Competing Interest

The authors declare that they have no known competing financial interests or personal relationships that could have appeared to influence the work reported in this paper.

Acknowledgments

This work was financially supported by the AZM & SAADE Association, the Lebanese University (Scientific research support program), the Lebanese Council of Scientific Research (CNRSL) and Bordeaux foundation. The authors thank Prof. Olivier Devos for valuable discussion on the EIS results.

Supplementary materials

Supplementary material associated with this article can be found, in the online version, at doi:10.1016/j.jma.2020.12.007.

References

[1] F. Dawood, M. Anda, G.M. Shafiullah, Int. J. Hydrogen Energy 45 (2020) 3847–3869, doi:10.1016/j.ijhydene.2019.12.059.
[2] JC. Radcliffe, The water energy nexus in Australia – The outcome of two crises, Water Energy Nexus 1 (2018) 66–85, doi:10.1016/j.wen.2018.07.003.
[3] M. Boudellal, Power-to-Gas: Renewable Hydrogen Economy for the Energy Transition, Walter de Gruyter GmbH & Co KG, 2018.
[4] D.A.J. Rand, J. Solid State Electrochem. 15 (2011) 1579–1622, doi:10.1007/s10008-011-1410-z.
[5] U. Sahaym, M.G. Norton, J. Mater. Sci. 43 (2008) 5395–5429, doi:10.1007/s10853-008-2749-0.
[6] D.J. Durbin, C. Malardier-Jugroot, Int. J. Hydrogen Energy 38 (2013) 14595–14617, doi:10.1016/j.ijhydene.2013.07.058.
[7] F. Mueller-Langer, E. Tzimas, M. Kaltschmitt, S. Peteves, Int. J. Hydrogen Energy 32 (2007) 3797–3810, doi:10.1016/j.ijhydene.2007.05.027.

[8] G. Marbán, T. Valdés-Solís, Int. J. Hydrogen Energy 32 (2007) 1625–1637, doi:10.1016/j.ijhydene.2006.12.017.
[9] A. Midilli, M. Ay, I. Dincer, M.A. Rosen, Renew. Sustain. Energy Rev. 9 (2005) 255–271, doi:10.1016/j.rser.2004.05.003.
[10] ES. Hanley, J.P. Deane, B.P. Ó Gallachóir, Renew. Sustain. Energy Rev. 82 (2018) 3027–3045, doi:10.1016/j.rser.2017.10.034.
[11] K. Mazloomi, C. Gomes, Renew. Sustain. Energy Rev. 16 (2012) 3024–3033, doi:10.1016/j.rser.2012.02.028.
[12] J.O. Abe, A.P.I. Popoola, E. Ajenifuja, O.M. Popoola, Int. J. Hydrogen Energy 44 (2019) 15072–15086, doi:10.1016/j.ijhydene.2019.04.068.
[13] M. Kalamaras, A.M. Efstathiou, in: Proceedings of the Conference Papers in Energy, 690627, 2013, 2013, doi:10.1155/2013/690627.
[14] J.D. Holladay, J. Hu, D.L. King, Y. Wang, Catal. Today 139 (2009) 244–260, doi:10.1016/j.cattod.2008.08.039.
[15] I. Dincer, C. Acar, Int. J. Hydrogen Energy 40 (2015) 11094–11111, doi:10.1016/j.ijhydene.2014.12.035.
[16] A. Konieczny, K. Mondal, T. Wiltowski, P. Dydo, Int. J. Hydrogen Energy 33 (2008) 264–272, doi:10.1016/j.ijhydene.2007.07.054.
[17] M. Balat, M. Balat, Int. J. Hydrogen Energy 34 (2009) 3589–3603, doi:10.1016/j.ijhydene.2009.02.067.
[18] Z.H. Tan, L.Z. Ouyang, J.M. Huang, J.W. Liu, H. Wang, H.Y. Shao, M. Zhu, J. Alloy. Compd. 770 (2019) 108–115, doi:10.1016/j.jallcom.2018.08.122.
[19] S.L. Li, J.M. Song, J.Y. Uan, J. Alloy. Compd. 772 (2019) 489–498, doi:10.1016/j.jallcom.2018.09.154.
[20] X. Hou, Yi Wang, Y. Yang, R. Hu, G. Yang, L. Feng, G. Suo, X. Ye, Li Zhang, H. Shi, Lu Yang, Z.G. Chen, Int. J. Hydrogen Energy 44 (2019) 24086–24097, doi:10.1016/j.ijhydene.2019.07.148.
[21] E. Alasmar, I. Aubert, A. Durand, M. Nakhl, M. Zakhour, E. Gaudin, J.L. Bobet, Int. J. Hydrogen Energy 44 (2019) 523–530, doi:10.1016/j.ijhydene.2018.10.233.
[22] Z. Tan, L. Ouyang, J. Liu, H. Wang, H. Shao, M. Zhu, Int. J. Hydrogen Energy 43 (2018) 2903–2912, doi:10.1016/j.ijhydene.2017.12.163.
[23] M. Ma, L. Yang, L. Ouyang, H. Shao, M. Zhu, Energy 167 (2019) 1205–1211, doi:10.1016/j.energy.2018.11.029.
[24] X.B. Xie, C. Ni, B. Wang, Y. Zhang, X. Zhao, Li Liu, B. Wang, W. Du, J. Alloy. Compd. 816 (2020) 152634, , doi:10.1016/j.jallcom.2019.152634.
[25] S. Al Bacha, A.S. Awad, E. El Asmar, T. Tayeh, J.L. Bobet, M. Nakhl, M. Zakhour, Int. J. Hydrogen Energy 44 (2019) 17515–17524, doi:10.1016/j.ijhydene.2019.05.123.
[26] J.Y. Uan, C.Y. Cho, K.T. Liu, Int. J. Hydrogen Energy 32 (2007) 2337–2343, doi:10.1016/j.ijhydene.2007.03.014.
[27] J.Y. Uan, M.C. Lin, C.Y. Cho, K.T. Liu, H.I. Lin, Int. J. Hydrogen Energy 34 (2009) 1677–1687, doi:10.1016/j.ijhydene.2008.11.097.
[28] J.Y. Uan, S.H. Yu, M.C. Lin, L.F. Chen, H.I. Lin, Int. J. Hydrogen Energy 34 (2009) 6137–6142, doi:10.1016/j.ijhydene.2009.05.133.
[29] S.H. Yu, J.Y. Uan, T.L. Hsu, Int. J. Hydrogen Energy 37 (2012) 3033–3040, doi:10.1016/j.ijhydene.2011.11.040.
[30] A.K. Figen, B. Coşkuner, S. Pişkin, Int. J. Hydrogen Energy 40 (2015) 7483–7489, doi:10.1016/j.ijhydene.2015.01.022.
[31] A.K. Figen, B.C. Filiz, Int. J. Hydrogen Energy 40 (2015) 16169–16177, doi:10.1016/j.ijhydene.2015.07.170.
[32] S. Al Bacha, S.A. Pighin, G. Urretavizcaya, M. Zakhour, F.J. Castro, M. Nakhl, J.L. Bobet, J. Power Sour. 479 (2020) 228711, doi:10.1016/j.jpowsour.2020.228711.
[33] S. Al Bacha, S.A. Pighin, G. Urretavizcaya, M. Zakhour, M. Nakhl, F.J. Castro, J.L. Bobet, Int. J. Hydrogen Energy 45 (2020) 20883–20893, doi:10.1016/j.ijhydene.2020.05.214.
[34] A.S. Awad, E. El-Asmar, T. Tayeh, F. Mauvy, M. Nakhl, M. Zakhour, J.L. Bobet, Energy 95 (2016) 175–186, doi:10.1016/j.energy.2015.12.004.
[35] S. Al Bacha, M. Zakhour, M. Nakhl, J.L. Bobet, Int. J. Hydrogen Energy 45 (2020) 6102–6109, doi:10.1016/j.ijhydene.2019.12.162.
[36] C. Wang, T. Yang, Y. Liu, J. Ruan, S. Yang, X. Liu, Int. J. Hydrogen Energy 39 (2014) 10843–10852, doi:10.1016/j.ijhydene.2014.05.047.
[37] M.H. Grosjean, L. Roué, J. Alloy. Compd. 416 (2006) 296–302, doi:10.1016/j.jallcom.2005.09.008.
[38] O.A. Buryakovskaya, M.S. Vlaskin, S.S. Ryzhkova, J. Alloy. Compd. 785 (2019) 136–145, doi:10.1016/j.jallcom.2019.01.003.
[39] A. Pardo, M.C. Merino, A.E. Coy, F. Viejo, R. Arrabal, S. Feliú, Electrochim. Acta 53 (2008) 7890–7902, doi:10.1016/j.electacta.2008.06.001.
[40] S. Candan, E. Candan, Trans. Nonferrous Met. Soc. China 27 (2017) 1725–1734, doi:10.1016/S1003-6326(17)60195-X.
[41] C. Ubeda, G. Garces, P. Adeva, I. Llorente, G.S. Frankel, S. Fajardo, Corros. Sci. 165 (2020,) 108384, , doi:10.1016/j.corsci.2019.108384.
[42] S. Al Bacha, I. Aubert, O. Devos, M. Zakhour, M. Nakhl, J.L. Bobet, Int. J. Hydrogen Energy 45 (2020) 15805–15813, doi:10.1016/j.ijhydene.2020.04.030.
[43] T. Tayeh, A.S. Awad, M. Nakhl, M. Zakhour, J.F. Silvain, J.L. Bobet, Int. J. Hydrogen Energy 39 (2014) 3109–3117, doi:10.1016/j.ijhydene.2013.12.082.
[44] ASTMStandard Practice for Codification of Certain Nonferrous Metals and Alloys Cast and Wrought, ASTM, 2005 B275-05.
[45] G.L. Song, A. Atrens, Adv. Eng. Mater. 1 (1999) 11–33, doi:10.1002/(sici)1527-2648(199909)1:1⟨11::Aid-adem11⟩3.0.Co;2-n.
[46] M.Y. Haciibrahimoğlu, M. Bedir, M. Öztaş, C. Cakez, Digest J. Nanomater. Biostruct. 10 (2015) 1439–1447 http://www.chalcogen.ro/1439_Haciibrahimoglu.pdf.
[47] C. Prakash, S. Singh, M. Kumar Gupta, M. Mia, G. Królczyk, N. Khanna, Materials 11 (2018) 1602 (Basel, Switzerland), doi:10.3390/ma11091602.
[48] Y. Liu, X. Wang, Z. Dong, H. Liu, S. Li, H. Ge, Mi Yan, Energy 53 (2013) 147–152. https://doi.org/10.1016/j.energy.2013.01.073
[49] Y. Liu, X. Wang, H. Liu, Z. Dong, G. Cao, Mi Yan, Energy 68 (2014) 548–554, doi:10.1016/j.energy.2014.01.005.
[50] D. Gan, Y. Liu, J. Zhang, Y. Zhang, C. Cao, Y. Zhu, L. Li, Int. J. Hydrogen Energy 43 (2018) 10232–10239, doi:10.1016/j.ijhydene.2018.04.119.
[51] I.B. Singh, M. Singh, S. Das, J. Magnes. Alloy. 3 (2015) 142–148, doi:10.1016/j.jma.2015.02.004.
[52] K. Gusieva, C.H.J. Davies, J.R. Scully, N. Birbilis, Int. Mater. Rev. 60 (2015) 169–194, doi:10.1179/1743280414Y.0000000046.
[53] E. Alasmar, 2018, « Systèmes ternaires à base de magnésium : synthèse, structure, propriétés physiques, stockage et/ou production d'hydrogène », PhD thesis, Université of Bordeaux and Lebanese University. http://www.theses.fr/2018BORD0023/document.
[54] M.H. Grosjean, M. Zidoune, L. Roué, J. Huot, R. Schulz, Electrochim. Acta 49 (2004) 2461–2470, doi:10.1016/j.electacta.2004.02.001.
[55] M. Esmaily, J.E. Svensson, S. Fajardo, N. Birbilis, G.S. Frankel, S. Virtanen, R. Arrabal, S. Thomas, L.G. Johansson, Prog. Mater. Sci. 89 (2017) 92–193, doi:10.1016/j.pmatsci.2017.04.011.
[56] F.H. Cao, V.H. Len, Z. Zhang, J.Q. Zhang, Rus. J. Electrochem. 43 (2007) 837–843, doi:10.1134/S1023193507070142.
[57] A.D. King, N. Birbilis, J.R. Scully, Electrochim. Acta 121 (2014) 394–406, doi:10.1016/j.electacta.2013.12.124.
[58] S. Al Bacha, A. Desmedt, M. Zakhour, M. Nakhl, J.L. Bobet, Electrochem. commun. 119 (2020) 106813, , doi:10.1016/j.elecom.2020.106813.
[59] D. Klotz, Electrochem. commun. 98 (2019) 58–62, doi:10.1016/j.elecom.2018.11.017.
[60] J.A.L. Dobbelaar, J.H.W. de Wit, J. Electrochem. Soc. 137 (1990) 2038–2046, doi:10.1149/1.2086861.
[61] P. Córdoba-Torres, Electrochim. Acta 225 (2017) 592–604, doi:10.1016/j.electacta.2016.12.087.
[62] P. Agarwal, J. Electrochem. Soc. 139 (1992) 1917, doi:10.1149/1.2069522.
[63] M.E. Orazem, B. Tribollet, Electrochemical Impedance Spectroscopy, John Wiley & Sons, 2017.
[64] S. Bender, J. Goellner, A. Heyn, S. Schmigalla, Mater. Corros. 63 (2012) 707–712, doi:10.1002/maco.201106225.
[65] J.N. Murray, P.J. Moran, E. Gileadi, Corrosion 44 (1988) 533–538, doi:10.5006/1.3583972.
[66] S. Li, D. Gan, Y. Zhu, Ya Liu, Ge Zhang, Li Li, Trans. Nonferrous Met. Soc. China 27 (2017) 562–568, doi:10.1016/S1003-6326(17)60062-1.